Vol. 63, No. 5, May 2007

ISSN 0143-974X

ELSEVIER

JOURNAL OF CONSTRUCTIONAL STEEL RESEARCH

Available online at www.sciencedirect.com
ScienceDirect

Journal of Constructional Steel Research 63 (2007) 581–590

JOURNAL OF CONSTRUCTIONAL STEEL RESEARCH
www.elsevier.com/locate/jcsr

Simulation of cold-formed steel beams in local and distortional buckling with applications to the direct strength method

Cheng Yu[a,*], Benjamin W. Schafer[b]

[a] *Department of Engineering Technology, University of North Texas, Denton, TX 76207, United States*
[b] *Department of Civil Engineering, Johns Hopkins University, Baltimore, MD 21218, United States*

Received 12 June 2006; accepted 25 July 2006

Abstract

A nonlinear finite element (FE) model is developed to simulate two series of flexural tests, previously conducted by the authors, on industry standard cold-formed steel C- and Z-section beams. The previous tests focused on laterally braced beams with compression flange details that lead predominately to local buckling failures, in the first test series, and distortional buckling failures, in the second test series. The objectives of this paper are to (i) validate the FE model developed for simulation of the testing, (ii) perform parametric studies outside the bounds of the original tests with a particular focus on variation in yield stress and influence of moment gradient on failures, and (iii) apply the study results to examine and extend the Direct Strength Method of design. The developed FE model shows good agreement with the test data in terms of ultimate bending strength. Extension of the tested sections to cover yield stresses from 228 to 506 MPa indicates that the Direct Strength Method is applicable over this full range of yield stresses. The FE model is also applied to analyze the effect of moment gradient on distortional buckling. It is found that the distortional buckling strength of beams is increased due to the presence of moment gradient. Further, it is proposed and verified that the moment gradient effect on distortional buckling failures can be conservatively accounted for in the Direct Strength Method by using an elastic buckling moment that accounts for the moment gradient. An empirical equation, appropriate for use in design, to predict the increase in the elastic distortional buckling moment due to moment gradient, is developed.

Keywords: Cold-formed steel; Finite element analysis; Local buckling; Distortional buckling; Direct strength method

1. Introduction

Laterally braced cold-formed steel beams generally suffer from one of two potential instabilities: local or distortional buckling. An extensive series of tests was conducted on industry standard cold-formed steel C and Z-beams to study local buckling (Yu and Schafer [1]) and distortional buckling (Yu and Schafer [2]) failures. Each test consisted of a pair of 5.5 m long C or Z-sections which were oriented in an opposed fashion and loaded at the 1/3 points along the length.

In the "local buckling tests" a through-fastened panel was attached to the compression flange, as shown in Fig. 1. The panel stabilized the compression flange, and specific fastener details were developed to avoid distortional buckling, but allow local buckling. In the "distortional buckling tests" nominally

Fig. 1. Local buckling test.

* Corresponding address: Department of Engineering Technology, University of North Texas, 3940 N. Elm St Room, F115F, Denton, TX 76207, United States. Tel.: +1 940 891 6891; fax: +1 940 565 2666.
E-mail address: cyu@unt.edu (C. Yu).

0143-974X/$ - see front matter © 2006 Elsevier Ltd. All rights reserved.
doi:10.1016/j.jcsr.2006.07.008

Fig. 2. Distortional buckling test.

identical specimens were tested, but the corrugated panel attached to the compression flange was removed in the constant moment region, so that distortional buckling could occur, as shown in Fig. 2.

The detailed nonlinear finite element model based on these two series of tests is fully summarized in Yu [3]. The validation work is briefly reviewed here, followed by two applications: (1) extension of the experimentally studied sections to examine the importance of yield stress variation on the solution; and (2) examination of the influence of moment gradient on distortional buckling of cold-formed steel beams.

2. Finite element modeling

2.1. Modeling details and loading/boundary conditions

An overall view of the developed FE model is provided in Fig. 3(a). The cold-formed steel beams, panel, and hot-rolled tubes, which stiffen the section at the load and support points, are modeled using 4-node, quadrilateral, shell elements (S4R in ABAQUS [4]). The ends of the beams are simply supported at the bottom flanges under the two circular tubes. Connection details and constraints on the sections, the hot-rolled steel tubes, the load beam, and the steel panel are illustrated in Fig. 3(b) and (c). "Link" constraints in ABAQUS are used to tie the tension flanges of the beams together at the location of the attached angles.

2.2. Geometric imperfections

Geometric imperfections of the tested beams were not measured. Therefore, the imperfections employed in the FE models were based on the statistical results by Schafer and Peköz [5]. We conservatively assumed that the Type 1 imperfection may be applied to the local buckling mode and the Type 2 imperfection applied to the distortional buckling mode, where Type 1 (d_1) imperfections are based on measured deviations from flat in the center of stiffened elements, and Type 2 (d_2) imperfections are based on measured deviations from flat at the edge of unstiffened elements or the flange/lip juncture of edge stiffened elements (see Schafer and Peköz [5]). For each test FE simulations were performed using imperfection magnitudes from the 25% and 75% values of the cumulative distribution function (CDF) of measured Type 1 and Type 2 imperfections. The first simulation used a larger initial geometric imperfection with a 75% CDF magnitude, or $d_1/t = 0.66$ for local buckling; $d_2/t = 1.55$ for distortional buckling. The second simulation used a smaller imperfection with a 25% CDF magnitude, or $d_1/t = 0.14$ for local buckling; $d_2/t = 0.64$ for distortional buckling. Thus, the two simulations cover the middle 50% of anticipated imperfection magnitudes. The final imperfection shape is a scaled superposition of the local and distortional buckling mode.

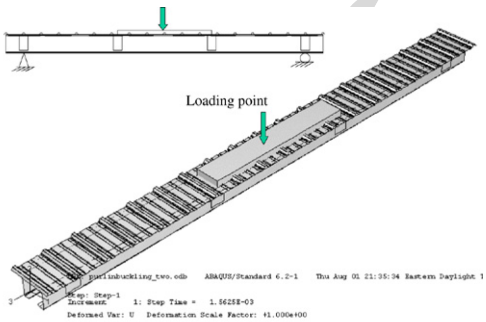

(a) Overall FE model.

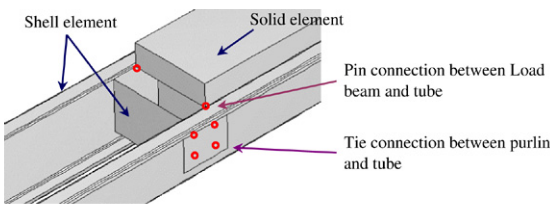

(b) Details at load point.

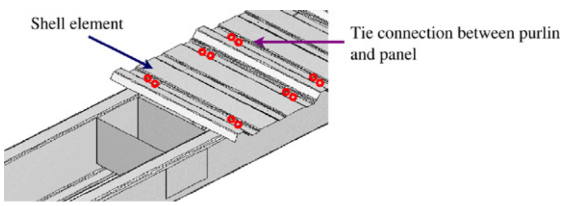

(c) Details at panel to section.

Fig. 3. Finite element modeling of beams in flexural tests.

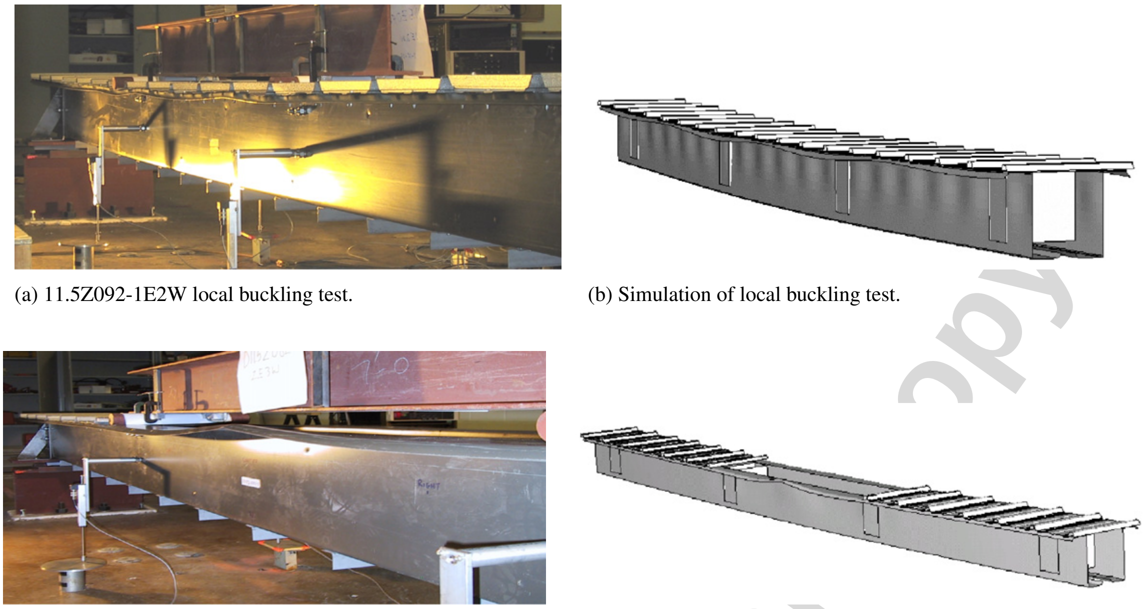

(a) 11.5Z092-1E2W local buckling test.

(b) Simulation of local buckling test.

(c) 11.5Z092-3E4W distortional buckling test.

(d) Simulation of distortional buckling test.

Fig. 4. General comparison of test and FE models.

2.3. Material modeling

Material nonlinearity in the cold-formed steel beams was modeled with von Mises yield criteria and isotropic hardening. Measured stress–strain relations taken from tensile coupons from the beams were employed. All other components were modeled as elastic, with $E = 203.4$ GPa and $\nu = 0.3$, except for the hot-rolled steel tubes and the loading beam which used an artificially elevated modulus (10E) so that they would effectively act as rigid bodies. Residual stresses were ignored. See Yu [3] for further discussion.

2.4. Nonlinear analysis method

The analysis of the ultimate strength of cold-formed steel members involves obtaining the nonlinear static equilibrium solution of an unstable problem. For such a problem, the generalized load–displacement response can exhibit non-monotonic response as the solution evolves. Simple incremental load or displacement algorithms fail to reproduce non-monotonic equilibrium paths and thus more robust methods are required. Among them, the modified Riks method (Crisfield [6]) has been proven both efficient and accurate, and is implemented in modern FE analysis codes such as ABAQUS. The Riks method is a variation of arc-length methods and may conceptually be understood as an incremental work solution. The Riks method has been employed with good success in past research on cold-formed steel members for finding the peak load (e.g., Schafer and Peköz [5]); however post-peak response may fail to converge, and the method is sensitive to step size and automatic incrementation algorithms (see Schafer [7]). In this research the method is augmented using artificial damping.

The addition of artificial damping is a technique for avoiding localized instabilities even in nonlinear static solutions (i.e., without performing a full dynamic analysis). Artificial damping is implemented in ABAQUS by adding mass-proportional damping of the form cM^*v to the global equilibrium equation: $P - I - cM^*v = 0$, where P is external forces, I is internal (nodal) forces, M^* is an artificial mass matrix calculated with unity density, c is the damping coefficient, $v = \Delta u/\Delta t$ and Δu is the increment of nodal displacements and Δt is the increment of time. The damping coefficient c is chosen such that, based on extrapolation of the results obtained during the first increment, the dissipated energy during the step is a small fraction of the change in strain energy during the step (2×10^{-4} by default). Unlike the definition of time in dynamics problems, the time in a nonlinear static analysis refers to increments of the total arc-length. Ideally, the damping is applied in such a way that the viscous forces are sufficiently large to prevent instantaneous buckling or collapse, but small enough not to affect the behavior significantly. This approach was employed to good success in this research.

2.5. Comparison with experimental results

As demonstrated in Fig. 4, the developed FE model provides a good prediction of the deformed shapes. The local buckling test is characterized by short and repeated buckling waves. The distortional buckling test failed with the compression flange rotating, and with a longer buckling wavelength than in the local mode.

Select load-to-deflection response of FE simulations are shown with comparison to the test results in Figs. 5 and 6. One measure of imperfection sensitivity is the difference in response between the 25% and 75% CDF values, as shown in the figures. Sensitivity to the peak strength is depicted by the vertical difference between the two curves at peak load, sensitivity to the final failure mechanism is also shown. For example, Fig. 5 shows a case where the peak load is sensitive to imperfection, but the failure mechanism, i.e. the response in the post-peak

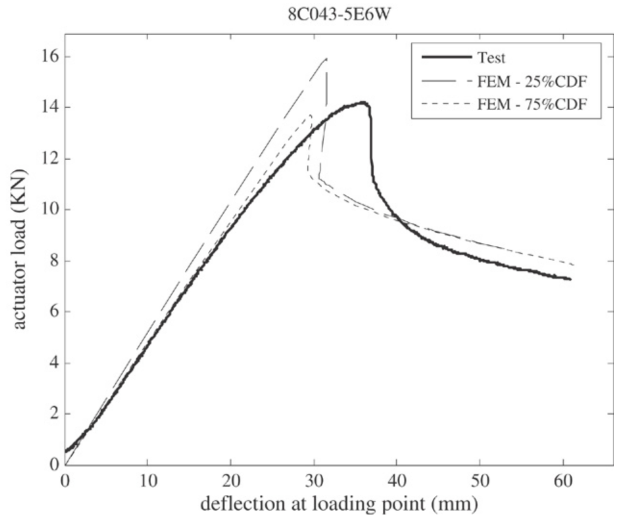

Fig. 5. Comparison of FEM results with test 8C043-5E6W.

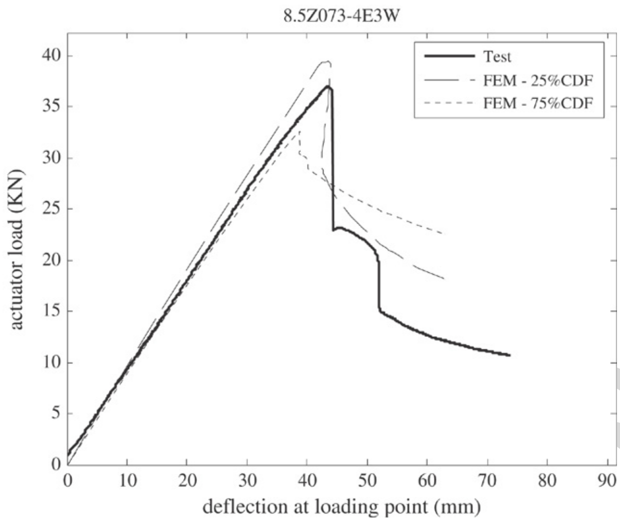

Fig. 6. Comparison of FEM results with test 8.5Z073-4E3W.

range appears nearly identical. Fig. 6 presents a case where post-peak mechanism response is clearly quite different for the two models. Many, but not all, cases exist where the post-peak slope predicted by the models is in qualitative agreement with the tests.

The results of the finite element analyses are summarized in Table 1 and Fig. 7. The mean response of the FE simulations has good agreement with the tested strength. The pair of simulations also provides a measure of imperfection sensitivity: the middle 50% of expected imperfection magnitudes result in a range of bending capacity equal to 13% for local buckling and 15% for distortional buckling.

Some limitations exist with the developed FE model. For example, a trend with respect to slenderness is observable (Fig. 7). This is likely due to our imperfection choice, which is a function of thickness (and thus is generally larger for the thicker, less slender, members). Further, the post-collapse mechanism is not always well approximated. Lack of agreement in the large deflection post-collapse range could be a function of the solution scheme (i.e., use of artificial damping instead of Riks) or more basic modeling assumptions, such as ignoring plasticity in the panels and the contact between components of the beam. Further discussion of the issues raised above and complete details of the modeling results may be found in Yu [3]. In total, it is concluded that the ultimate strength for both local buckling and distortional buckling of cold-formed steel beams is well simulated by this finite element model, and thus the model is considered to be validated and is used for further study in this paper.

3. Application I: Extended finite element analysis and application of the direct strength method

Given the successful verification of the developed finite element model, extension to a greater variety of cold-formed steel sections and material properties (not examined experimentally) is possible. Of particular interest is a further examination of yield stress on the behavior. This was primarily driven by the fact that experimentally measured yield stress for the tested Z-sections showed little variation, but for the C-sections covered an extensive range. A subset of the tested sections, covering yield stresses from 228 to 506 MPa, and with stress–strain curves based on experimentally measured coupons, was employed in this parametric study. The FE results from these models are then compared with the Direct Strength Method (NAS [8], Schafer and Peköz [9]).

Models of both the local buckling test and distortional buckling test (no panel attached to the compression flange in the pure bending region) were completed. A subset of the tested geometries was selected, as given in Table 2. The notations in Table 2 refer to Fig. 8. The primary focus for experimental examination was on Z-sections since they are more prone to distortional buckling and little variation in yield stress. The method of generating geometric imperfections described in the previous section was again employed. A single maximum imperfection magnitude corresponding to the 50%

Table 1
Summary of finite element analysis results for local buckling tests

	Test label	$P_{25\%\sigma}/P_{\text{test}}$	$P_{75\%\sigma}/P_{\text{test}}$	$P_{\text{mean}}/P_{\text{test}}$
Local buckling tests	Mean	1.06	0.93	1.00
	Standard deviation	0.06	0.07	0.06
Distortional buckling tests	Mean	1.08	0.93	1.01
	Standard deviation	0.07	0.07	0.06

Note: P_{test}: Peak tested actuator load; P_{mean}: approximated by average value of $P_{25\%\sigma}$: and $P_{75\%\sigma}$; $P_{25\%\sigma}$: Peak load of simulation with 25% CDF of maximum imperfection; $P_{75\%\sigma}$: Peak load of simulation with 75% CDF of maximum imperfection.

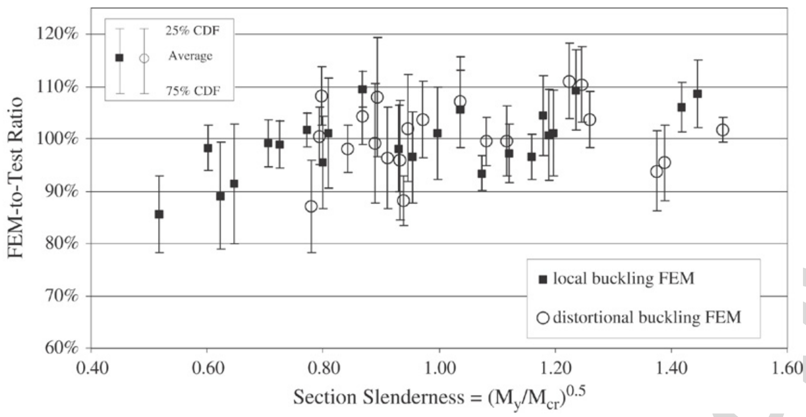

Fig. 7. Accuracy and sensitivity of FE predictions for tested beams.

Table 2
Geometry and yield stress[a] of analyzed sections

Specimen	h (mm)	b_c (mm)	d_c (mm)	θ_c (deg)	b_t (mm)	d_t (mm)	θ_t (deg)	r_{hc} (mm)	r_{dc} (mm)	r_{ht} (mm)	r_{dt} (mm)	t (mm)
8Z2.25 × 050	194.4	55.9	21.9	50.0	55.9	21.9	50.0	5.8	5.8	5.8	5.8	1.215
8Z2.25 × 100	194.4	55.9	21.9	50.0	55.9	21.9	50.0	5.8	5.8	5.8	5.8	1.215
8.5Z2.5 × 70	206.6	60.8	21.9	50.0	60.8	21.9	50.0	6.1	6.1	6.1	6.1	1.701
8.5Z092	204.1	63.2	21.9	51.8	58.3	24.3	50.4	6.8	6.8	7.5	7.5	2.187
8.5Z120	206.6	63.2	24.3	47.8	60.8	24.3	48.9	8.8	8.8	8.3	8.3	2.858
8.5Z082	205.6	60.8	23.1	49.0	57.4	23.6	50.3	6.8	6.8	7.3	7.3	1.959
11.5Z3.5 × 80	279.5	85.1	21.9	50.0	85.1	21.9	50.0	7.3	7.3	7.3	7.3	1.944
8C068	192.0	46.2	17.0	80.0	48.6	14.6	77.8	3.9	3.9	3.9	3.9	1.701
8C097	195.4	50.8	14.1	85.1	50.3	12.9	86.3	6.8	6.8	7.1	6.8	2.381
12C068	291.6	48.6	14.6	85.0	48.6	14.6	85.0	6.3	6.6	6.3	6.3	1.652

[a] Yield stress, $f_y = 228, 303, 387, 429, 506$ MPa.

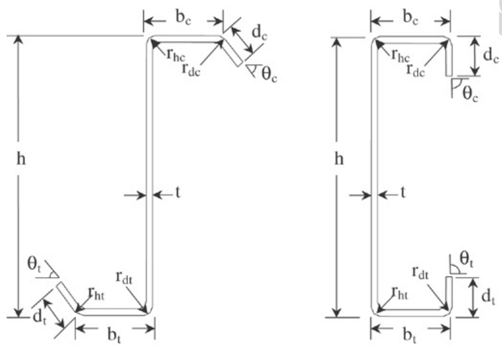

Fig. 8. Definitions of specimen dimensions for Z and C sections.

CDF magnitude: $d_1/t = 0.34$ for local buckling mode; $d_2/t = 0.94$ for distortional buckling mode, was selected.

3.1. The performance of the direct strength method

Fig. 9(a) shows a comparison of the local buckling strength of cold-formed steel beams calculated by the Direct Strength Method (DSM) with data from both the tests and the extended FE simulations. A similar comparison for distortional buckling is provided in Fig. 9(b). Table 3 summarizes the comparison of DSM predictions with both the tested and extended FE model bending capacities. In general, DSM provides reliable and conservative predictions for the bending strength of cold-formed steel beams. The local buckling strength predictions are more scattered than those of distortional buckling, and significant inelastic reserve is ignored.

Table 3
Summary of DSM predictions vs. test and FEM results

		Local buckling		Distortional buckling	
		M_n/M_{DSM}	Number	M_n/M_{DSM}	Number
Tests	μ	1.03	23	1.01	18
	σ	0.06	23	0.07	18
FEM	μ	1.02	50	1.04	50
	σ	0.07	50	0.07	50
Overall	μ	1.03	73	1.03	68
	σ	0.07	73	0.07	68

Note: μ — average; σ — standard deviation; M_n — bending capacity of beams (test or ABAQUS); M_{DSM} — predictions of direct strength method; Number — the number of analyzed sections.

4. Application II: Moment gradient effect on distortional buckling

The second application for the developed FE model is related to the influence of moment gradients on the member strength. In practical situations beams are subjected to a variety of moment gradients. In design, moment gradient is considered

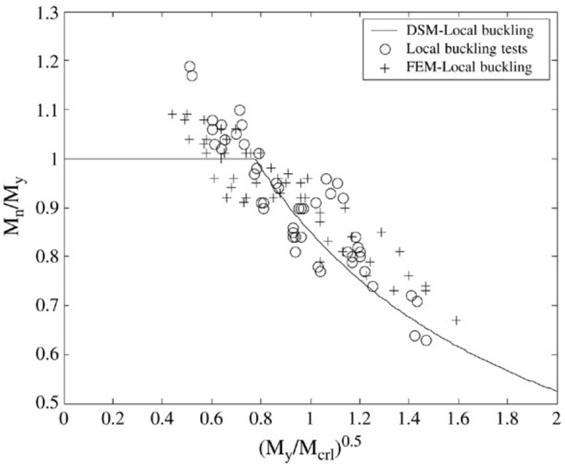

(a) Local buckling strength.

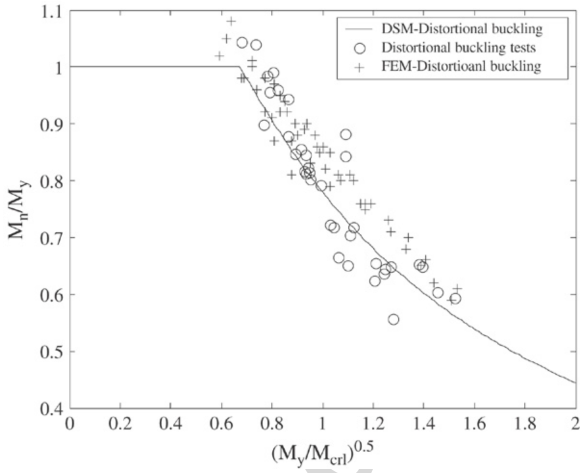

(b) Distortional buckling strength.

Fig. 9. Comparison of DSM to tests and extended FE results.

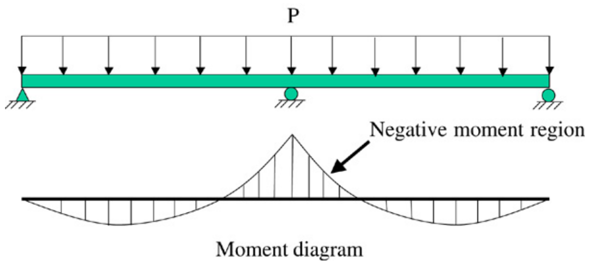

Fig. 10. A continuous beam under uniform distributed loads.

in the calculation of lateral-torsional buckling (i.e., C_b) but ignored in local and distortional buckling. In the local mode the buckling half-wavelength is short and the moment gradient has only a minor influence (particularly for stiffened elements, see Yu and Schafer [10,11]). However, in the distortional mode the buckling half-wavelength is long enough that typical moment gradients can have influence. This issue is of some practical significance, because one common case for concern in distortional buckling is the negative bending region of a continuous beam: Fig. 10. Significant moment gradients exist in this region, and in practice little restraint may be placed on the compression/bottom flanges.

In this section, the moment gradient effect on both elastic buckling and ultimate strength of cold-formed steel beams failing in distortional buckling is analyzed by FE simulation.

4.1. Elastic distortional buckling under moment gradient

First, the moment gradient effect on the elastic distortional buckling moment (M_d) of cold-formed steel beams is explored. For example, see the work of Bebiano et al. [12]. Here, an FE model (in ABAQUS) is utilized to determine M_d under a linear moment gradient, r (where $r = M_1/M_2$, M_1 and M_2 are the end moments, $|M_2| > |M_1|$). The developed FE model is shown in Fig. 11(a), along with the resulting elastic distortional buckling modes under varying moment gradients: Fig. 11(b)–(d).

Twelve typical cold-formed steel C and Z-sections are chosen for detailed elastic distortional buckling FE analysis, see Table 4. For the selected sections the influence of linear moment gradient (r) on the elastic distortional bucking moment (M_d) of a beam of fixed length ($L = 3L_{\text{crd}}$) is shown in Fig. 12; where, L_{crd} is the half-wavelength and M_{crd} is the elastic buckling moment for distortional buckling under constant moment ($r = 1$). The elastic distortional buckling moment is increased when a moment gradient is applied. For example, when $r = -1$ (double curvature) a 30%–50% increase is observed.

Fig. 12 shows that moment gradient has an influence on elastic distortional buckling, but if the same moment gradient occurs over a longer length of the beam this influence will dissipate. For a triangular bending moment diagram ($r = 0$) this dissipation is illustrated in Fig. 13. Theoretically, as $L \to \infty$, the buckling moment will converge to the case with no moment gradient (i.e., M_{crd}), but the FE analysis indicates convergence to these limiting values is slow. For beams with a length of $10L_{\text{crd}}$, a minimum 10% increase in M_d above M_{crd} is still observed. A lower bound of the moment gradient effect for $r = 0$ is:

$$M_d/M_{\text{crd}} = 1.0 \leq 1.0 + 0.4\left(\frac{L_{\text{crd}}}{L}\right)^{0.7} \leq 1.3. \tag{1}$$

The moment gradient factor r, and section length ratio L_{crd}/L, are two essential parameters for representing the moment gradient influence. An "equivalent moment concept" is proposed here as an approximate method to simplify the possible loading configurations (different r and L_{crd}/L) to a single case, as shown in Fig. 14(a) and (b). The equivalent moment concept presumes that the elastic distortional buckling moment of a beam with length L and moment gradient $r = M_1/M_2$ is equal to the elastic distortional buckling moment of the same section with length L_e under moment gradient $r = 0$.

A series of finite element analyses were performed to examine the equivalent moment concept. Three cases were studied: (1) $L = 3L_{\text{crd}}$, $r = 0$; (2) $L = 1.5L_{\text{crd}}$, $r = 0.5$; (3) $L = 4.5L_{\text{crd}}$, $r = -0.5$. The equivalent moment concept presumes that these three cases have the same elastic distortional buckling moment (i.e., M_d based on $L_e = 3L_{\text{crd}}$,

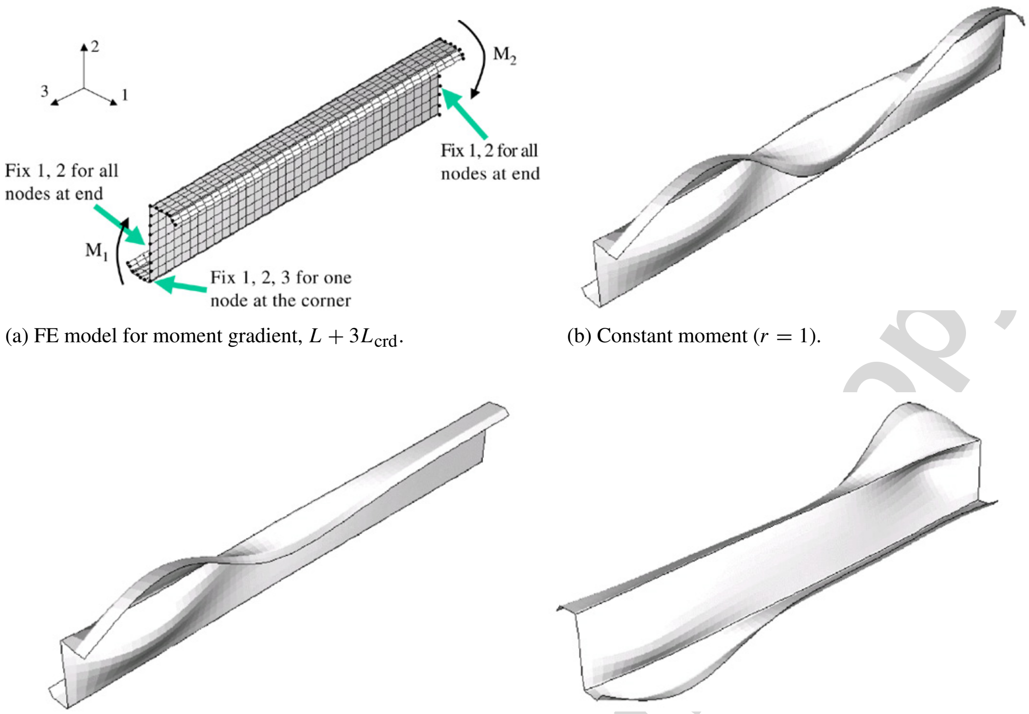

(a) FE model for moment gradient, $L + 3L_{\text{crd}}$.

(b) Constant moment ($r = 1$).

(c) Linear moment gradient ($r = 0$).

(d) Double curvature ($r = -1$).

Fig. 11. FE model and distortional buckling of Z-section subjected to moment gradient.

Table 4
Geometry of selected sections for study

Type	Label	h (mm)	b_c (mm)	d_c (mm)	θ_c (deg)	b_t (mm)	d_t (mm)	θ_t (deg)	r_{hc} (mm)	r_{dc} (mm)	r_{ht} (mm)	r_{dt} (mm)	t (mm)
Z	8Z50	203.2	57.2	23.6	50.0	57.2	23.6	50.0	6.1	6.1	6.1	6.1	1.270
	8Z100	203.2	57.2	23.6	50.0	57.2	23.6	50.0	6.1	6.1	6.1	6.1	2.540
	11.5Z100	292.1	88.9	22.9	50.0	88.9	22.9	50.0	7.6	7.6	7.6	7.6	2.540
	8.5Z070	215.9	63.5	22.9	50.0	63.5	22.9	50.0	6.4	6.4	6.4	6.4	1.778
	8.5Z082	214.9	63.5	24.1	49.0	59.9	24.6	50.3	7.1	7.1	7.6	7.6	2.047
	8.5Z120	215.1	65.8	24.4	47.8	62.5	25.4	48.9	9.1	9.1	8.6	8.6	2.987
	8.5Z092	214.1	66.3	23.4	51.8	61.0	24.1	50.4	7.1	7.1	7.9	7.9	2.286
	11.5Z080	292.1	88.9	22.9	50.0	88.9	22.9	50.0	7.6	7.6	7.6	7.6	2.032
C	8C097	204.2	53.1	14.7	85.1	52.6	13.5	86.3	7.1	7.1	7.4	7.1	2.489
	8C054	203.2	52.1	15.0	89.4	51.8	14.2	83.3	5.6	5.8	5.8	6.1	1.321
	10C068	256.5	52.6	13.5	80.7	52.8	13.2	81.9	6.1	5.8	5.8	5.6	1.610
	3.62C054	94.7	47.8	10.4	87.0	47.5	10.9	89.0	6.6	6.1	6.9	6.9	1.410

$r = 0$). The FE results are summarized in Table 5, and it is shown that the distortional buckling moment of these three cases, for each section, are indeed quite close; the error is below 3% on average. The equivalent moment concept is a simplification with validity, at least for the studied sections.

Using the equivalent moment concept, all moment gradient effects can be projected to the same case in which a moment gradient $r = 0$ is applied to the beam with the equivalent length L_e, and Eq. (1) can be generalized to:

$$M_d/M_{\text{crd}} = 1.0 \le 1 + 0.4(L_{\text{crd}}/L)^{0.7} \times (1 - M_1/M_2)^{0.7} \le 1.3 \qquad (2)$$

where M_2 and M_1 are the end moments on a segment of beam of length L; $|M_2| > |M_1|$, single curvature is positive;
L_{crd} is the half wavelength of distortional buckling under constant moment ($M_1 = M_2$);
M_{crd} is the distortional buckling moment under constant moment ($M_1 = M_2$);
M_d is the distortional buckling moment under a moment gradient $r = M_1/M_2$ ($M_1 \neq M_2$).

4.2. Ultimate distortional buckling strength under moment gradient

In this section, the previously validated nonlinear FE model is extended to investigate ultimate strength in distortional buckling under a moment gradient. Two nonlinear FE models were used in the investigation. The first model, Fig. 15, modifies

Table 5
Finite element results for verifying equivalent moment concept

Section label	M_{crd-1} (kip-in.) ($r = 0$, $L = 3L_{crd}$)	M_{crd-2}/M_{crd-1} ($r = 0.5$, $L = 1.5L_{crd}$)	M_{crd-3}/M_{crd-1} ($r = -0.5$, $L = 4.5L_{crd}$)
8Z50	73.33	1.02	0.99
8Z100	323.13	1.03	0.99
11.5Z100	342.36	1.03	1.00
8.5Z070	150.34	1.04	1.00
8.5Z082	205.23	1.03	0.99
8.5Z120	451.59	1.03	1.00
8.5Z092	257.51	1.03	0.99
11.5Z080	213.73	1.02	1.00
8C097	317.85	1.04	0.94
8C054	80.78	1.03	0.99
10C068	115.94	0.97	0.95
3.62C054	45.74	1.03	1.00
	Average	1.03	0.99

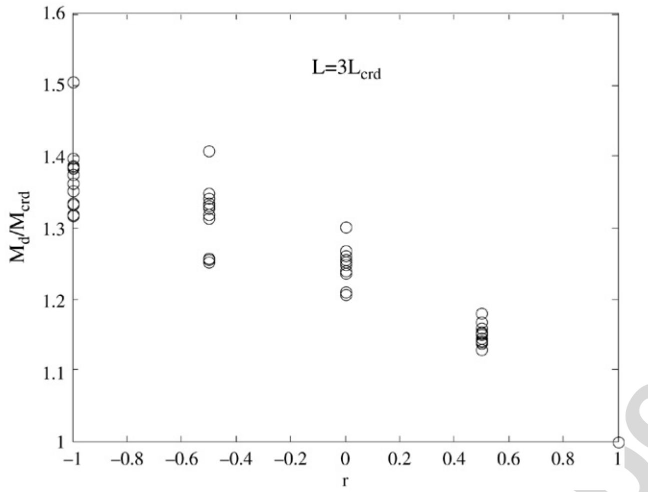

Fig. 12. Moment gradient ($r = M_1/M_2$) influence on elastic distortional buckling.

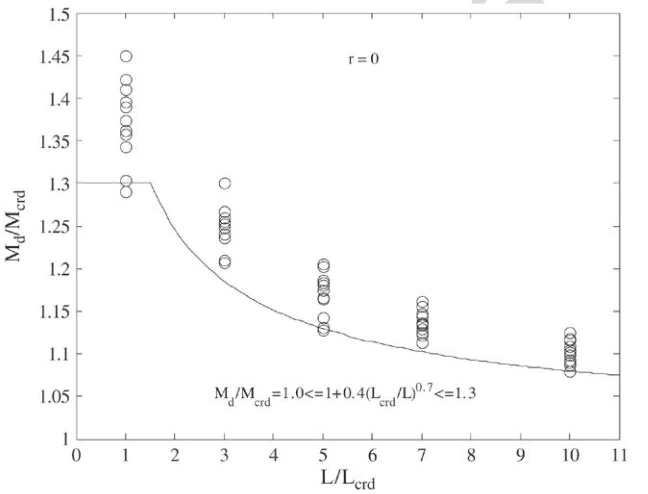

Fig. 13. Section length ratio influence on elastic distortional buckling.

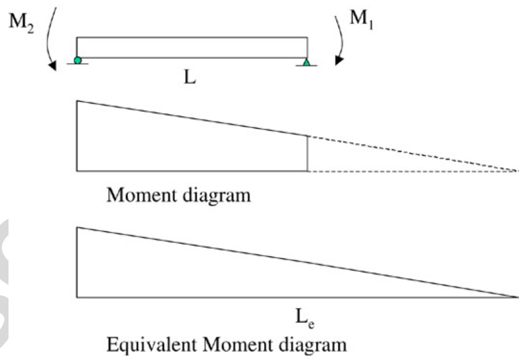

(a) Single curvature.

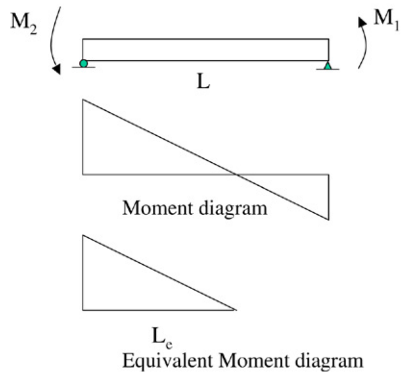

(b) Double curvature.

Fig. 14. Equivalent moment concept for elastic distortional buckling prediction.

the original test setup to a single load P applied at the first 1/3 point, thus the unrestrained part of the beam is subjected to a moment gradient $r = 0.5$. The second model, Fig. 16, replaces the constant moment region with a single midspan applied load and braces the compression flange with corrugated panel on one side only, thus the beam is subjected to a moment gradient $r = 0$. A local and distortional buckling combined mode shape is selected for the initial geometric imperfection, and the magnitude corresponds to the 50% CDF. Yield stresses of 228, 303, 387, 429, and 506 MPa based on tensile coupons taken from earlier tested specimens are employed.

Fig. 15 shows the deformed shape of beam 11.5Z080 subjected to a moment gradient, $r = 0.5$, analyzed by the first finite element model, the material yield stress is 429 MPa. A

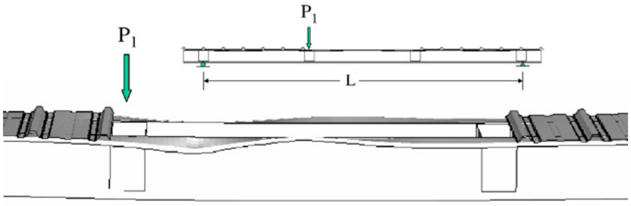

Fig. 15. Deformed shape of 11.5Z080 beam subjected to moment gradient $r = 0.5$.

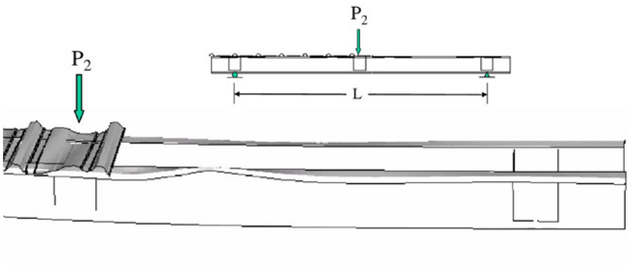

Fig. 16. Deformed shape of 8.5Z070 beam subjected to moment gradient $r = 0$.

distortional buckling wave is observed close to the load point where maximum bending moment exists. The finite element analysis shows the bending capacity of this beam is increased 15% when the moment gradient $r = 0.5$ is applied.

Fig. 16 illustrates the deformed shape of beam 8.5Z070 subjected to a moment gradient $r = 0$, analyzed by the second finite element model. The distortional buckling half-wave forms next to the load point and the finite element analysis indicates that the strength of the beam is increased 22.5% compared with the same beam under constant moment.

The geometry of the C- and Z-sections analyzed by the two FE models is given in Table 6. The numerical results are summarized in Table 7, where it is shown that when compared to simulations of the distortional buckling tests under constant moment, the bending strength in the distortional buckling mode increases by an average of 15% (see $M_{FEd\text{-}MG}/M_{FEd}$) due to the presence of the moment gradient.

It is proposed that the influence of the moment gradient on the strength may be approximated in the Direct Strength Method by allowing the elastic buckling moment M_{crd} in the Direct Strength Method equations to include the influence of moment gradient; i.e., let M_d of the previous section be used in place of M_{crd}. The consequence of this choice is shown in Fig. 17, where M_d of Eq. (2) has been used in place of M_{crd} — the result is a conservative approximation to the strength increase observed due to the moment gradient. If the exact M_d is used instead of Eq. (2), the resulting strength prediction ($M*_{DSd\text{-}MG}$ of Table 7) is slightly improved. Comparison of the accuracy of the Direct Strength equations for distortional buckling failures without moment gradient, Fig. 9(b), to that of Fig. 17 indicates that while the proposed approach is simple, it remains a bit on the conservative side. Indicating that post-buckling and collapse under the moment gradient may be slightly different than in constant moment, an issue that deserves further study.

Table 6
Geometry of analyzed C and Z-sections

Specimen	h (mm)	b_c (mm)	d_c (mm)	θ_c (deg)	b_t (mm)	d_t (mm)	θ_t (deg)	r_{hc} (mm)	r_{dc} (mm)	r_{ht} (mm)	r_{dt} (mm)	t (mm)
8.5Z082	214.9	63.5	24.1	49.0	59.9	24.6	50.3	7.1	7.1	7.6	7.6	2.047
8.5Z120	215.1	65.8	24.4	47.8	62.5	25.4	48.9	9.1	9.1	8.6	8.6	2.987
11.5Z080	292.1	88.9	22.9	50.0	88.9	22.9	50.0	7.6	7.6	7.6	7.6	2.032
8C097	204.2	53.1	14.7	85.1	52.6	13.5	86.3	7.1	7.1	7.4	7.1	2.489
8.5Z070	215.9	63.5	22.9	50.0	63.5	22.9	50.0	6.4	6.4	6.4	6.4	1.778
8Z100	203.2	57.2	23.6	50.0	57.2	23.6	50.0	6.1	6.1	6.1	6.1	2.540
11.5Z100	292.1	88.9	22.9	50.0	88.9	22.9	50.0	7.6	7.6	7.6	7.6	2.540
8Z050	203.2	57.2	23.6	50.0	57.2	23.6	50.0	6.1	6.1	6.1	6.1	1.270

Table 7
Comparisons of DSM predictions with FE results

		$M_{FEd\text{-}MG}/M_{FEd}$	$M*_{DSd\text{-}MG}/M_{DSd}$	$M_{FEd\text{-}MG}/M_{DSd\text{-}MG}$	$M_{FEd\text{-}MG}/M*_{DSd\text{-}MG}$
FE model with $r = 0.5$	μ	1.13	1.06	1.15	1.14
	σ	0.02	0.03	0.05	0.05
FE model with $r = 0$	μ	1.25	1.07	1.22	1.20
	σ	0.04	0.02	0.04	0.04
Overall	μ	1.15	1.06	1.16	1.15
	σ	0.05	0.03	0.06	0.05

Note: μ — average; σ — standard deviation; $M_{FEd\text{-}MG}$ — FE prediction of ultimate moment in distortional buckling with moment gradient; M_{FEd} — FE prediction of ultimate moment in distortional buckling no moment gradient; $M*_{DSd\text{-}MG}$ — Direct strength prediction of nominal moment in distortional buckling, with M_{crd} determined by FE elastic buckling including moment gradient influence; $M_{DSd\text{-}MG}$ — Direct strength prediction of nominal moment in distortional buckling, with M_{crd} determined from Eq. (2) and includes moment gradient influence; M_{DSd} — Direct Strength prediction of nominal moment in dist. buckling no moment gradient.

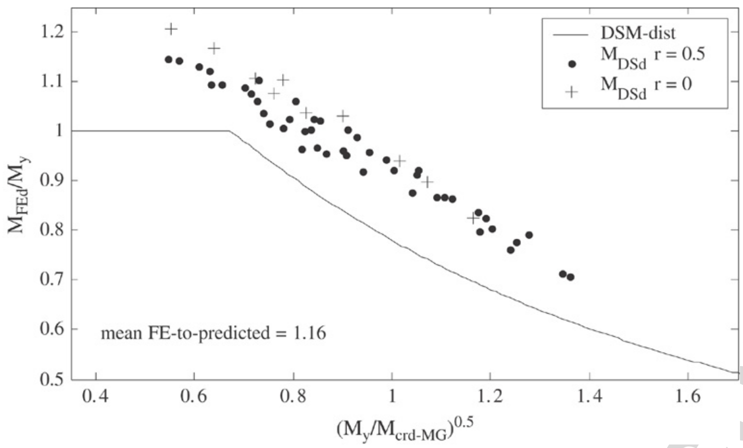

Fig. 17. Comparison of the direct strength method distortional buckling prediction with finite element modeling ($M_{\text{crd-}MG} = M_d$ of Eq. (2)).

5. Conclusions

A nonlinear FE model was developed (in ABAQUS) and verified against previously conducted flexural tests on cold-formed steel C- and Z-section beams. The FE analysis was extended to beams not included in the tests; in particular, yield stress was varied from 228 to 506 MPa. The results indicate that the Direct Strength Method yields reasonable strength predictions for both local and distortional bucking failures of Z and C-section beams with a wide range of industry standard geometries and yield stresses of steel. The FE model was also utilized to study the distortional buckling and post-buckling behavior of cold-formed steel beams under moment gradient. Moment gradients were achieved by applying a single concentrated load in the middle of simply supported beams. The FE results show that overly conservative predictions will be made if the moment gradient effect is ignored in distortional buckling. It is also shown that by using the appropriate elastic buckling moments, the Direct Strength Method is a conservative predictor of the increased strength due to moment gradient in distortional buckling. The elastic distortional buckling moment under a moment gradient can be determined by finite element analysis, or by the empirical equation proposed in the paper, Eq. (2).

References

[1] Yu C, Schafer BW. Local buckling tests on cold-formed steel beams. Journal of Structural Engineering 2003;129(12):1596–606.
[2] Yu C, Schafer BW. Distortional buckling tests on cold-formed steel beams. Journal of Structural Engineering 2006;132(4):515–28.
[3] Yu C. Distortional buckling of cold-formed steel members in bending. Ph. D. dissertation. Baltimore (MD): Johns Hopkins University; 2005.
[4] ABAQUS. ABAQUS Version 6.2. Pawtucket (RI): ABAQUS, Inc; 2001. http://www.abaqus.com.
[5] Schafer BW, Peköz T. Computational modeling of cold-formed steel: Characterizing geometric imperfections and residual stresses. Journal of Constructional Steel Research 1998;47(3):193–210.
[6] Crisfield MA. A fast incremental/iteration solution procedure that handles 'snap-through'. Computers and Structures 1981;13:55–62.
[7] Schafer BW. Cold-formed steel behavior and design: Analytical and numerical modeling of elements and members with longitudinal stiffeners. Ph. D. dissertation. Ithaca (NY): Cornell University; 1997.
[8] NAS. Appendix 1 of the North American specification for the design of cold-formed steel structural members. Washington (DC): American Iron and Steel Institute; 2004.
[9] Schafer BW, Peköz T. Direct strength prediction of cold-formed steel members using numerical elastic buckling solutions. In: Proceeding of the fourteenth international specialty conf on cold-formed steel structures. 1998. p. 69–76.
[10] Yu C, Schafer BW. Stress gradient effect on the buckling of thin plates. In: Proceedings of the seventeenth international specialty conf on cold-formed steel structures. 2004. p. 47–70.
[11] Yu C, Schafer BW. Stability of thin plates under longitudinal stress gradients. In: Annual technical session and meeting. Structural Stability Research Council. 2006. p. 405–24.
[12] Bebiano R, Silvestre N, Camotim D. On the influence of stress gradients on the local-plate, distortional and global buckling behavior of thin-walled steel members. In: Annual tech. session and meeting. Structural Stability Research Council. 2006. p. 301–27.